Final Technical Report

1. Award Number: **G13AP00033**

2. Title of Award: **Earthquake Size and Slip Rate of the Pyramid Lake Fault Zone near Reno, Nevada**

3. Authors

Stephen Angster[1,2], Weiliang Huang[3], Steven Wesnousky[1,2], Graham Kent[2], Takashi Nakata[4], and Hideaki Goto[4]
University of Nevada, Reno
[1]Center for Neotectonics Studies
[2]Nevada Seismological Laboratory
MS 174 MS169
1664 N Virginia St.
Reno, Nevada 89557
[3]Institute of Geology, China Earthquake Administration, Beijing, China
[4]Hiroshima University, Japan
Dept. of Geography
[1]775-784-6067, Fax: none
[1]sangster@nevada.unr.edu and wesnousky@unr.edu
[2]gkent@unr.edu
[3]haungweiliang1987@gmail.com

4. Principal Investigators **Graham Kent[2] and Steven Wesnousky[1,2]**

5. Term of Award: **June 1, 2013 – August 31, 2014**

Abstract

The report herein describes the methods and observations acquired during the length of this award concerning the slip rate and coseismic properties of the Pyramid Lake fault zone. The Pyramid Lake fault zone is a well-developed northwest trending right-lateral fault in the northern Walker Lane, located ~30 km east of Reno, NV. Previous paleoearthquake and slip rate studies indicate that the Pyramid Lake fault has produced 3 surface rupturing paleoearthquakes since 8980 ± 260 cal. Yr B.P. and has an average minimum slip rate of ~2.6 ± 0.3 mm/yr since the late Pleistocene. Reconciling these observations implies that coeseismic offset must have averaged ~7 to 9 meters, much larger than would generally be expected from empirical scaling relationships for a strike-slip fault of its 45 km length. In this study, we use high-resolution modeling techniques to document previously unobserved observations of right laterally displaced geomorphic features along the northern section of the Pyramid Lake fault. With these eight new displacement measurements that range from 16.1 – 24.4 meter of right lateral displacement and using chronologic constraints provided by previous lake level studies of lake Lohantan, we determine a new independent slip rate of 1.0 ±0.3 mm/yr and interpret that coseismic displacements along the fault have ranged from 4-6 meters. These values are consistent with geodetically determined slip rates that fall within the expected range from empirically derived scaling relations of maximum coseismic displacements.

Publications resulting from the work

Angster, S., Haung, W., Wesnousky, S., Kent, G., 2014, Reevaluation of the Pyramid Lake Fault Zone Slip Rate: Integrating High-Resolution Datasets from LiDAR, Drone Photography, and Aerial Photographs, SSA Annual Conference 2014, 14-507.

Report

Introduction

The Pyramid Lake fault zone is a well-developed northwest trending right-lateral fault in the northern Walker Lane (Anderson and Hawkins, 1984; Bell and Slemmons, 1979; Briggs and Wesnousky, 2004), Figure 1. Previous paleoearthquake and slip rate studies indicate that the Pyramid Lake fault has produced 3 surface rupturing paleoearthquakes since 8980 ± 260 cal. Yr B.P. and has an average minimum slip rate of ~2.6 ± 0.3 mm/yr since the late Pleistocene (Briggs and Wesnousky, 2004). Reconciling these observations implies that coeseismic offset should have averaged ~7 to 9 meters, much larger than would generally be expected from empirical scaling relationships for a strike-slip fault of its 45 km length (Wells and Coppersmith, 1994; Wesnousky, 2008). Evidence of repeated offsets of this size has not been recorded or recognized along the length of the fault. High-resolution surface modeling holds the potential to further address this conundrum.

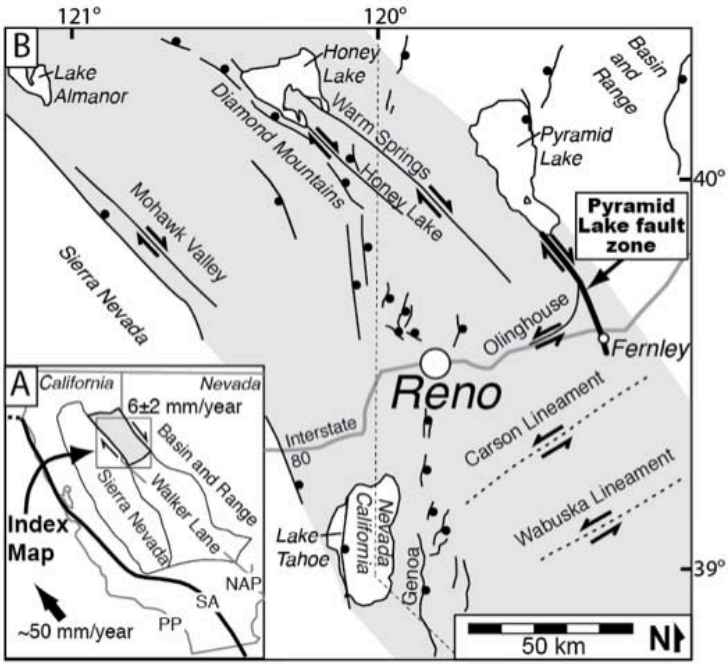

Figure 1. (A) Small scale map of the Walker Lane and the San Andreas (SA) fault system. (B) Large scale map of northern Walker Lane and associated major faults. (Figure is from Briggs and Wesnousky, 2004).

Here we present new observations of tectonically displaced geomorphic features along the Pyramid Lake fault acquired from high-resolution (<20 cm) digital elevation models (DEMs). The models are developed from aerial imagery taken from a remote controlled multi-rotor hobby copter processed with Agisoft Photoscan software©, a method previously described as Structure from Motion (Westoby et al., 2012). After further describing the methods of our analysis, we follow with description of our observations and the bearing of these observations on the slip rate and coseismic behavior of the Pyramid Lake fault.

Methods

Initially, we attempted to use Terrestrial based LiDAR data (Maptek, iSite 8800) to develop high-resolution models along the Pyramid Lake fault. However, due to the presence of relatively dense sagebrush cover and the nature of the low angle of incidence that the scanner has with the ground, we found the terrestrial LiDAR scanner to be ineffective for such a large area.

To overcome the challenges of the terrestrial LiDAR, we applied SfM to low altitude aerial photography obtained from a low flying remote controlled multi-rotor hobby copter. Our modeling procedures are described below. Because this is a relatively new technique, especially towards geomorphology, we first provide a general summary of SfM.

Structure from Motion

Sprouting from stereo-photogrammetry, SfM developed during the late 1970's (Ullman, 1977, 1979), and has since rapidly progressed into simple automated workflows that produce highly accurate 3-D point data comparable to models produced from standard LiDAR (Harwin and Lucieer, 2012; Westoby et al., 2012). Applications have ranged from modeling iconic solitary structures (Snavely et al., 2008), mountainous landscapes and outcrops (Westoby et al., 2012), to geomorphic landscapes (Fonstad et al., 2013; Johnson et al., 2014).

SfM uses standard photogrammetric triangulation of common features from a set of photographs, that have overlapping coverage from different multiple perspectives, to produce high-density 3-D point data (Figure 2). Scene geometry and texture is recreated from enhanced feature recognition algorithms that allow for multi-scaled photographs to have large changes in camera perspectives. Feature color is also carried through the SfM process, providing red-green-blue values for each derived point and creating texture to the model. Recent applications and testing of SfM for topographic modeling show high levels of accuracies that are often comparable and sometime better than standard LiDAR models (Fonstad et al., 2013; Harwin and Lucieer, 2012; Johnson et al., 2014; Westoby et al., 2012).

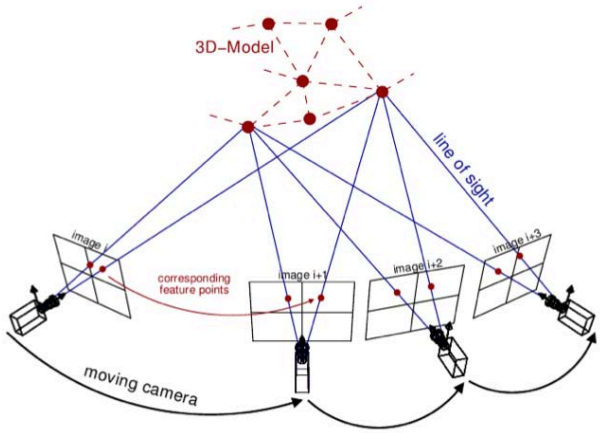

Figure 2. Conceptual model of Structure from Motion.

For our models, we followed very similar procedures to (Johnson et al., 2014) using Agisoft Photoscan software©. Generated point clouds were gridded at maximum ground resolution quality described in Table 1, and processed into raster surfaces. Next, hillshade and contour maps were produced using ESRI ArcGIS tools from which our measurements were made.

Model	Model Area (square meters)	Number of Images	GCPs	Point Density (points/square meter)	Ground Resolution (cm/pixel)
A	189,278	971	43	130.1	**4**
B	101,181	326	11	238.3	**6.5**
C	143,615	352	11	126.0	**8.9**
D	78,432	88	18	1158.6	**2.9**
E	445,386	558	10	121.1	**9**
F	230,591	350	8	109.4	**9.5**
G	131,812	381	14	206.2	**6.9**
H	122,681	338	7	166.8	**7.7**

Table 1. Structure from Motion modeling results.

Pyramid Lake fault Surface Trace and Offset Potential

The Pyramid Lake fault is expressed as a relatively narrow fault zone that extends for ~45 km from Fernley, NV to the southern edge of Pyramid Lake, where it continues along the shoreline (Eisses et al., in review) for another ~40 km (Figure 3). Previous geomorphic and structural mapping of this fault have divided it into two sections (Anderson and Hawkins, 1984; Bell and Slemmons, 1979; Bell et al., 2005; Briggs and Wesnousky, 2004). The southern section of the Pyramid Lake fault extends from south Fernley, NV to where the Olinghouse fault merges (Figure 3). Along this section of the fault zone, it is expressed as multiple discontinuous linear traces manifested as vegetation lineaments, scarps, and linear depressions commonly paralleling the Truckee River. At the northern extent of the southern section, the Pyramid Lake fault displays local extensional characteristics associated with the interaction of the conjugate left-lateral Olinghouse fault (Briggs and Wesnousky, 2005; Sanders and Slemmons, 1996). The northern section of the Pyramid Lake fault is the most well defined and displays a nearly continuous long linear fault trace manifested as vegetation lineaments, uphill-facing scarps, bedrock and alluvial ridges, elongate depressions,

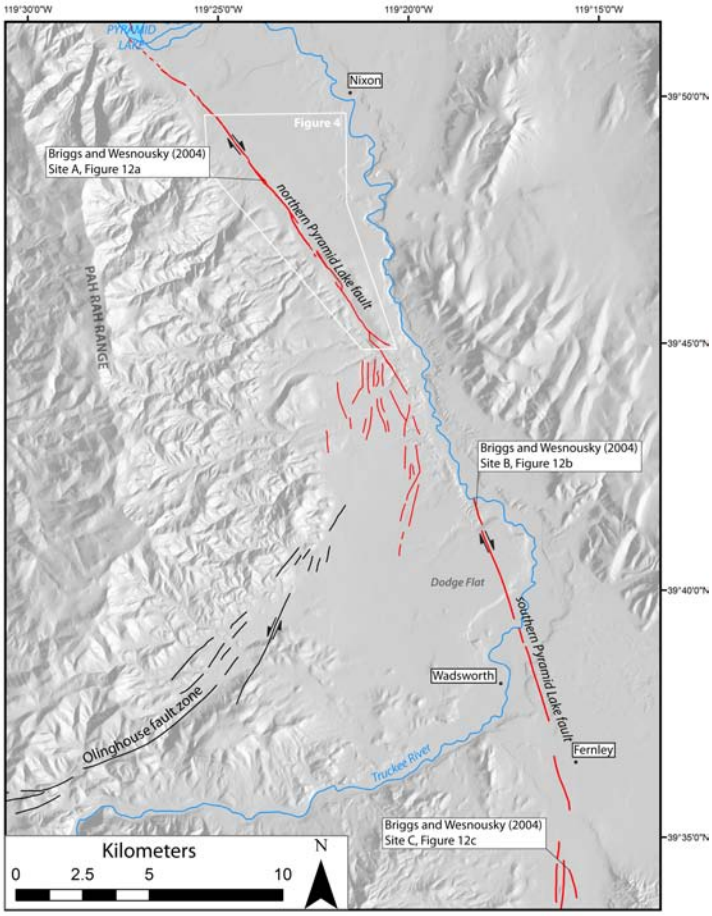

Figure 3. Map of the Pyramid Lake fault zone with respect to Pyramid Lake, the Truckee River, and the Olinghouse fault zone. Previous slip rate site of Briggs and Wesnousky (2004) are shown.

and springs (Figure 3 and 4). This portion of the fault crosses numerous gullies and channels and was chosen for study because it provides the highest potential in the geomorphology for extracting displacement measurements.

High-Resolution Hobby Copter Models

We developed seven surface models, labeled A-H in Figure 4, of geomorphic units that afforded the highest potential to record displacements of geomorphic features offset by fault displacement. Low altitude (< 30 meters) aerial photographs were acquired at each site using a DJI Phantom 1 multi-rotor hobby copter mounted with a 5.9 mm Ricoh GR 8.3 megapixel digital camera. Photo capture was focused along the trace of the fault, which allowed for the most photo overlap and thus produced the highest ground resolution along the fault. During flight, images were captured every 5 seconds producing ~100–950 photographs at each site. Poor quality photos such as those that were blurred, contained obstructions, and were taken at very low altitude were disregarded from the modeling process.

Ground Control Points (GCPs) were deployed before photo acquisition. These consisted of orange 30 cm diameter disks set up in rows of 3 perpendicular to the fault, spaced ~50 meters apart. Targets were geospatially located using a Trimble differential GPS.

Observations

Geomorphic Units and Age Control

The Pyramid Lake basin was once part of Lake Lohantan, a pluvial lake that reached is maximum highstand of ~1337 m at 13,070 ±60 ^{14}C B.P. (15,475 ±720 cal. Yr B.P.) before rapidly desiccating to what is now Pyramid Lake (Adams et al., 1999; Benson and Thompson, 1987; Briggs et al., 2005). Remnant shoreline features such as shoreline scarps, spits, and tufa deposits are prevalent within Pyramid Lake basin and provide excellent late Pleistocene and Holocene geomarkers, from which

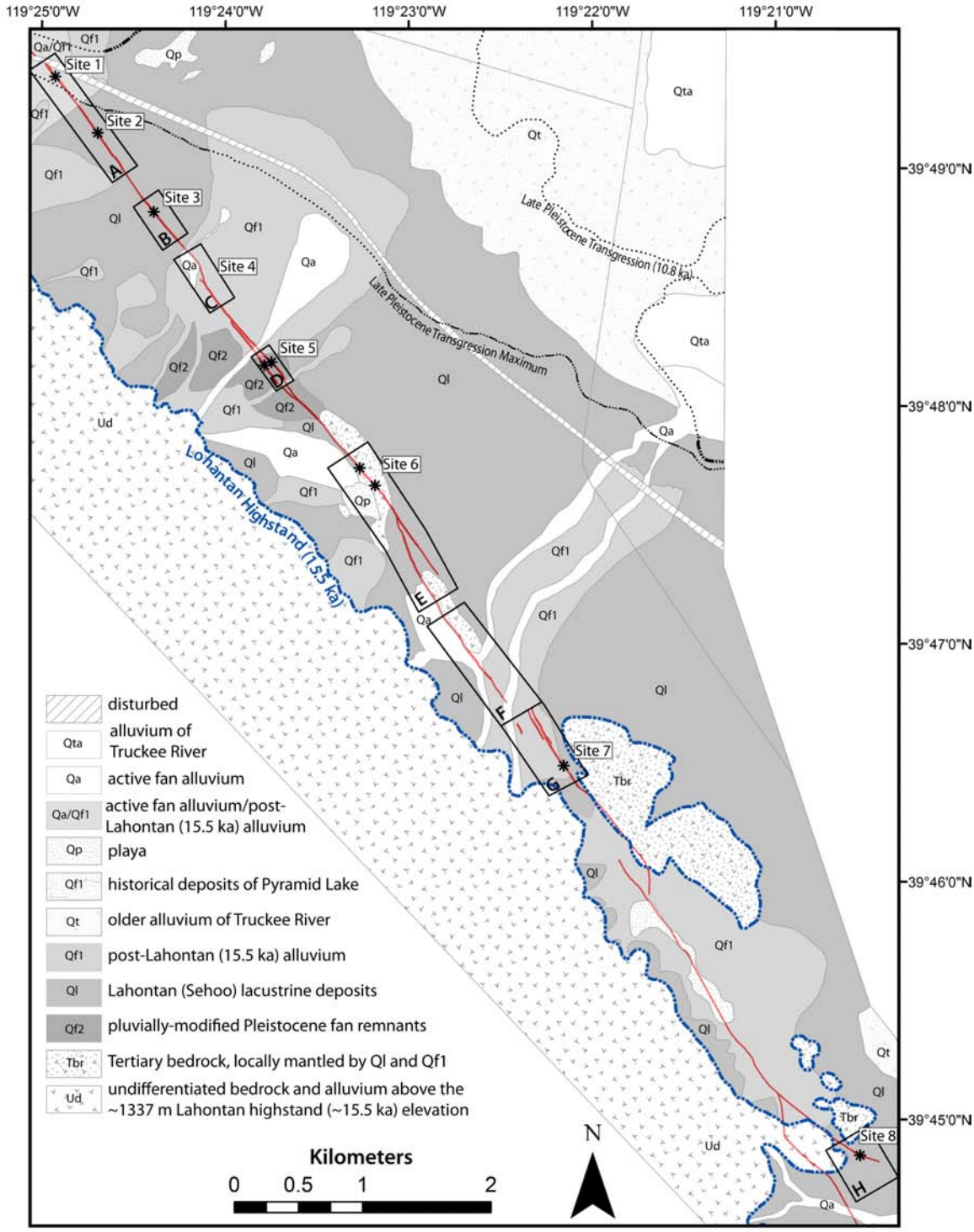

Figure 4. Modified surficial map of the northern section of the Pyramid Lake fault from Briggs and Wesnousky (2004). Lohantan highstand is marked by blue dotted line and black dashed lines indicate late Pleistocene transgressions. Black rectangles outline the extent of high-resolution models. Offset measurement sites are marked with an asterisk.

detailed lake-level curves have been generated (Adams, 2012; Adams et al., 1999; Benson and Thompson, 1987; Briggs et al., 2005).

The trace of the Pyramid Lake fault zone lies almost entirely below the highstand. The age of the highstand thus bounds the maximum age of offset geomorphic deposits that lie along this section of the fault (15.5 ka) (Figure 4). Additionally, at one site, the fault locally interacts with deposits of younger and lower lake transgressions that reached elevations of 1199 m (2635 ± cal yr BP) and 1230 m (10,820 ±35 cal yr BP)(Briggs and Wesnousky, 2005).

Offset Observations

From the seven models produced along the fault, eight sites display an apparent right lateral offset of various geomorphic features (Figure 4). Each site was analyzed and all but Site 4 were determined as real tectonic offset. These are described in the following:

Site 1

Offset Site 1 is located at the northern end of the study area (Figure 4). Here, the trace of the Pyramid Lake fault is expressed as a single linear uphill facing scarp (~0.25 m) within a post-Lahontan highstand alluvial fan (Qa/Qf1) (Figure 4). The surface of this fan unit is characterized by a relatively dense network of through-going shallow (< 0.25 m) and narrow ephemeral drainage channels. The interfluves have uneven surfaces and are covered by sparsely spaced low sagebrush.

Site 1 sits at an elevation of ~1238 m, which is just above the late-Pleistocene transgressional maximum (1230 m)(Briggs and Wesnousky, 2005). The absence of shoreline features on the surface of this alluvial fan (Qa/Qf1) implies that the alluvial fan post-dates the late Pleistocene transgression (10,820 ±35 BP).

The hillshade model displays a clear linear expression of the fault and of the drainages across the fan (Figure 5a). Along the trace of the fault, we observe a beheaded drainage channel and a possible parental channel on the opposite side of the fault. From a 25 cm contour map, we traced the thalwegs of these channels and measured a horizontal right-lateral offset of ~16.7 meters. Given that this amount

of displacement has accrued since the deposition of the alluvial fan unit (Qa/Qf1), which post-dates the 10,820 ka transgression; we determine a maximum slip-rate of 1.5 mm/yr at this site.

a)

b)

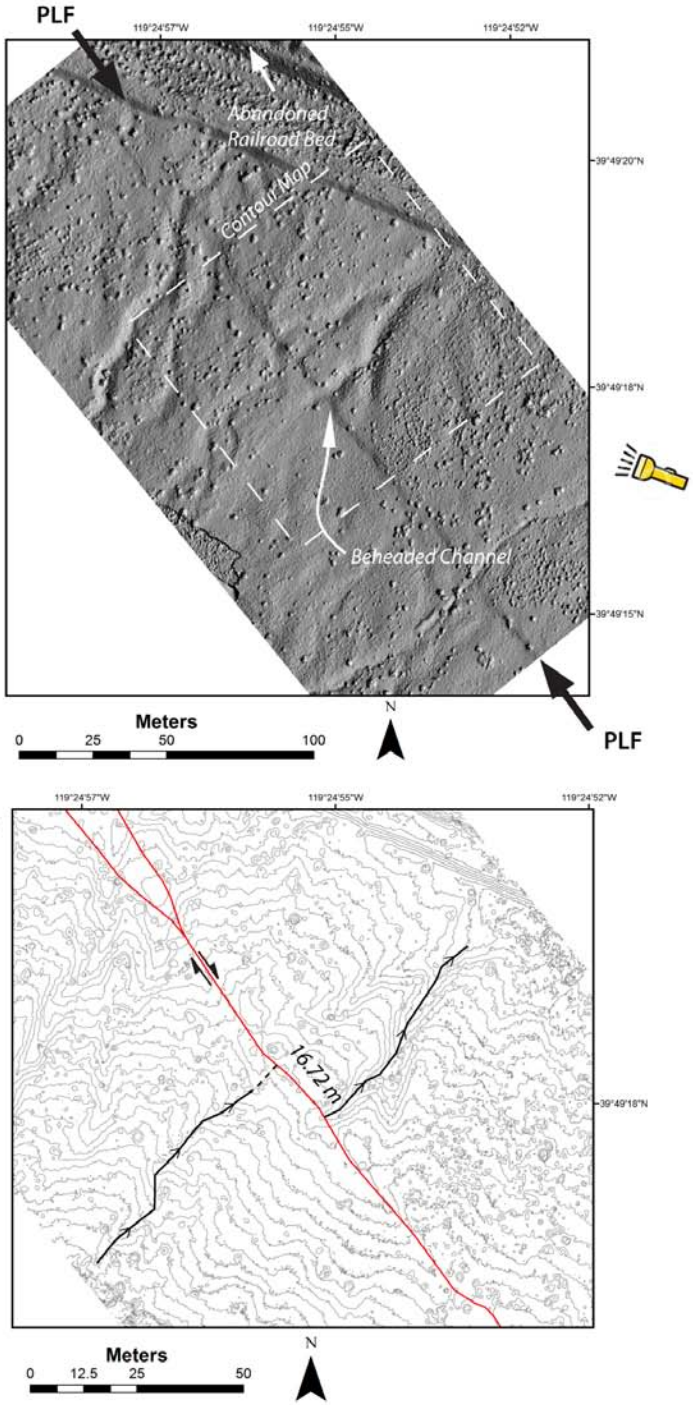

Figure 5. High-resolution model of offset Site 1. a) hillshade model of site showing beheaded channel. b) 25cm contour map showing displacement measurement of offset thalwegs (traced with black solid and dotted line).

Site 2

Offset Site 2 is also located near the northern end of the study region where the Pyramid Lake fault is expressed as a single linear relatively large uphill facing scarp (~1.5 m) that parallels the mountain front within lacustrine deposits (Ql) (Figure 4). The surface of this unit is relatively smooth, gently sloping, and is incised by deep (~3-8 meters) abandoned drainages.

The model produced at this site includes one of these drainages and intersects the fault and displays an apparent right-lateral offset (Figure 6). Using a 25 cm contour map, we estimate the right lateral offset of the channel thalweg to be on the order of ~24.2 meters. The measurement is coupled with significant uncertainty because the channel margin on the southwest side of the fault becomes poorly defined as it approaches the fault. Furthermore, a secondary younger drainage system, running

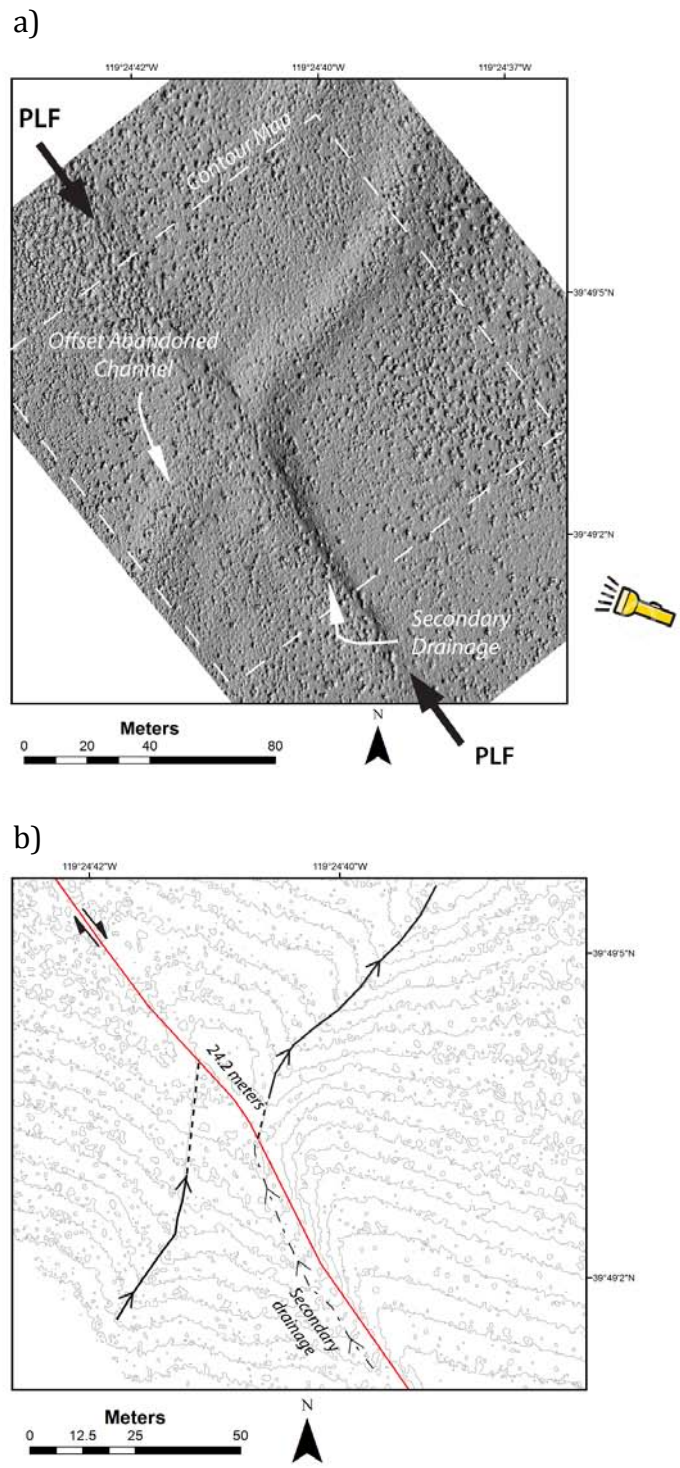

Figure 6. High-resolution model of offset Site 2. a) hillshade model of site showing right laterally offset channel. b) 25cm contour map showing displacement measurement of offset thalwegs (traced with black solid and dotted line).

parallel to the fault scarp, interferes with the channel morphology where it meets the fault and further obscures measurement. A conservative estimate of the offset measurement is judged to be about/on the order of ~5 meters.

This site sits well below the Lahontan highstand and has thus accrued since ~ 15.5 ka. Using this as the maximum age of this deposit, we determine a maximum slip rate of 1.5 mm/yr at this site.

Site 3

Site 3 is located about ~0.75 km to the southeast of Site 2 and displaces lacustrine deposits Ql interpreted to be the same age as at Site 2 (Figures 4). Here, a broad constructional shoreline ridge intersects the trace of the Pyramid Lake fault at an oblique angle. The digital elevation model and accompanying 25 cm contour map is interpreted to reflect ~16.16 meters of right lateral displacement to have occurred since the ridge was formed (Figure 7). The broad nature of the shoreline ridge and obliqueness of the ridge to the fault of course imparts significant uncertainty to our measurement. As seen at Site 2, the formation of the shoreline feature is estimated to post-date the Lahontan highstand (~15.5 ka) and, along with the offset measurement, implies a slip rate of ~1.0 mm/yr at this site.

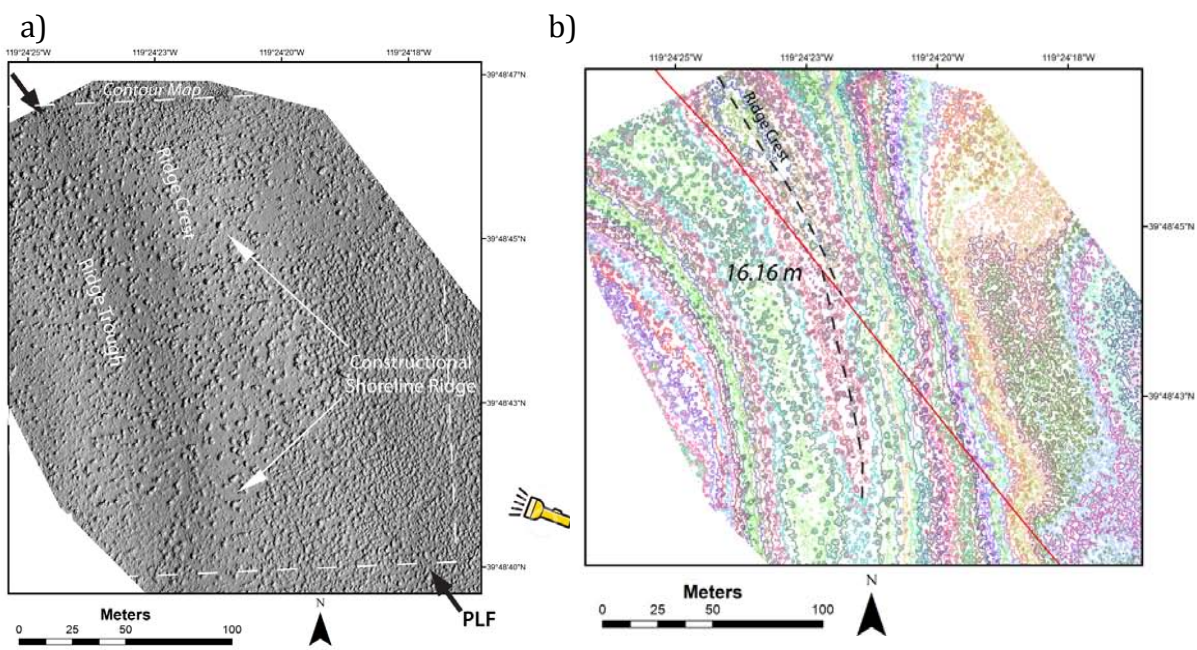

Figure 7. High-resolution model of offset Site 3. a) hillshade model of site showing constructional shoreline feature. b) 25cm contour map showing displacement measurement of ridge crests (traced with black dashed line). Contours are randomly color to assist in differentiating contours.

a)

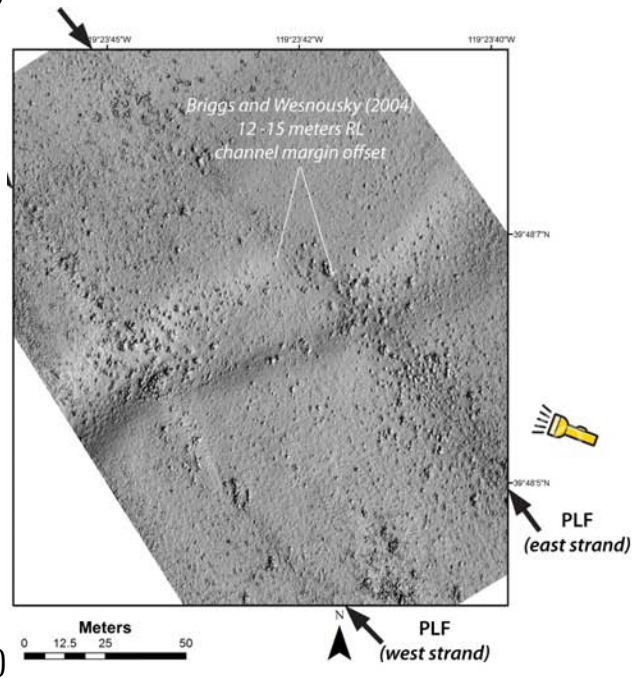

b)

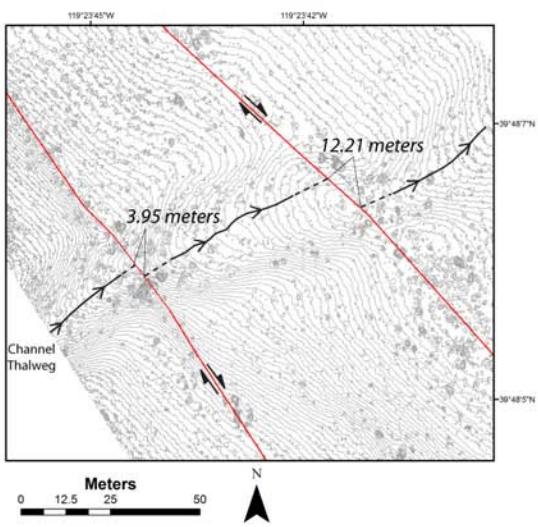

Figure 8. High-resolution model of offset Site 5. a) hillshade model of site showing offset drainage and two surface traces of PLF. b) 25cm contour map showing displacement measurement of offset thalwegs on each fault trace (traced with black solid and dotted line).

Site 5

Site 5 is located near the middle of the study area where the Pyramid Lake fault is expressed as two fault strands and forms a graben structure across a pluvially modified fan (Qf2) (Figures 4 and 8). Here, the Pyramid Lake fault offsets an abandoned drainage channel previously identified by (Briggs and Wesnousky, 2004). They observed the northern channel margin is right-laterally offset 12-15 m since the highstand of pluvial Lake Lahontan on the eastern fault strand and noted the offset may be explained by a minimum slip rate of 0.7 – 1 mm/yr. No measureable offset was reported on the western strand. Their measurement is duplicated with the 25 cm contour map we have constructed to better illustrate the trace the thalweg of the channel. We measure 12.2 m of right lateral displacement of the thalweg. We also observe channel offset on the western fault strand, and measure ~3.9 m of right lateral displacement.

Our measurement on the eastern strand falls within the range of the (Briggs and Wesnousky, 2004) measurement and has minimal obstructions, in terms of measurement. The newly observed measurement the western strand, however, is

obstructed by large sagebrush yielding an ~1.5 m of uncertainty to our measurement.

Due to the absence of geomorphic features, it is difficult to detect whether these displacements occurred independently or coseismically. Either way, the sum of the two displacements (16.1 m) represents the total amount of offset at this site that has developed since the development of the channel, which post-dates the Lahontan highstand (15.5 ka). The sum total of observations yields a slip rate estimate of 1.0 mm/yr at this site.

Site 6

Site 6 is located at the southern end of a long (~1 km) linear NW trending fault bound and wave-washed bedrock ridge (Figures 4). Here, two constructional shorelines strike southwestward across the strike of the fault (Figure 9).

We traced the crest of these shoreline ridge features using a 25 cm contour map, and measure a 21.5 m right lateral displacement on the northern ridge and a 20.4 m right lateral displacement of the southern ridge crests.

The lacustrine ridge features are close in elevation to one-another and assumed to be similar in age. The amount of measured displacement on each is quite comparable, and likely represents the accumulation of the same number of earthquake events. The difference in measured displacements is for this reason interpreted to represent an uncertainty in the offset measurement. Again using the age of the Lohantan highstand as a bound on the age of displacement, we determine a slip rate of 1.3 ±0.1 mm/yr at this site.

Site 7

Site 7 is ~2.5 km southeast of Site 6, located on the south side of an active alluvial fan that covers the trace of the fault (Figure 4). Here the Pyramid Lake fault is expressed as a single uphill facing scarp within Qf1 and Ql deposits (Figure 4). Sets of lacustrine shoreline scarps that sit just below the Lahontan highstand (~1337 m) intersect the Pyramid Lake fault at a high angle and show right lateral offset (Figure 10).

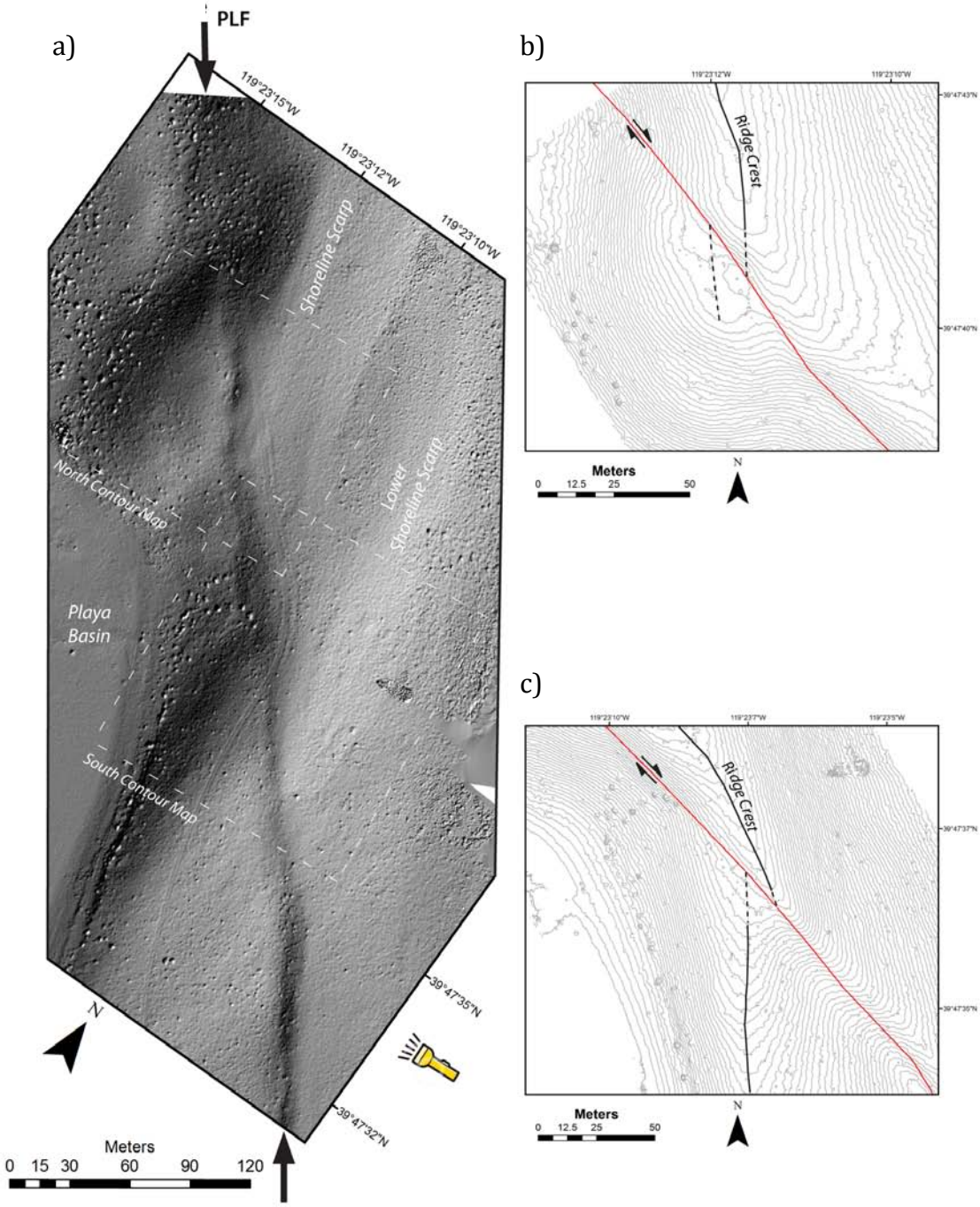

Figure 9. High-resolution model of offset Site 6. a) hillshade model of site showing offset shoreline features. b and c) 25cm contour maps of northern (b) and southern (c) offset shoreline features. Solid and dotted black lines show trace of ridge crests.

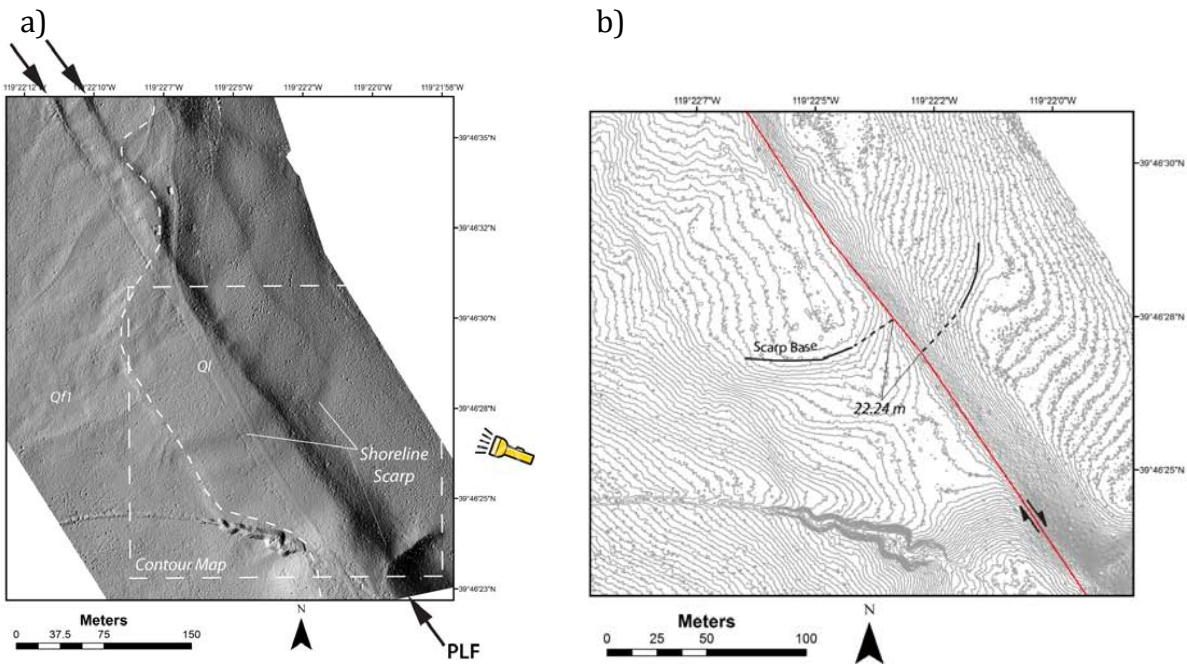

Figure 10. High-resolution model of offset Site 7. a) hillshade model of site showing uphill facing scarp and intersecting shoreline scarps. b) 25cm contour map showing displacement measurement of shorelines (traced with black solid and dotted line).

We project the steepest inflection of the northwest slope of the scarps into the fault trace and measure ~22.2 m of right-lateral displacement across the fault. Assuming that this offset has accrued since the highstand (15.5 ka), we determine a slip rate of 1.4 mm/yr.

Site 8

Offset site 8 is located at the southern end of the study area at the southern end of a linear bedrock ridge (Figure 4). Here, shoreline scarps wrap around the southern tip of the ridge and intersect the fault trace (Figure 11). Tracing and projection of the base of the scarps into the fault trace reveals ~21.3 m of right lateral offset.

At this location, the Pyramid Lake fault forms a wide distributed fault zone of multiple surface traces as a result of interaction with the Holocene active Olinghouse Fault zone to the west (Briggs and Wesnousky, 2005; Sanders and Slemmons, 1996). Our observed offset measurement is on the eastern most mapped

fault trace. Because of this, our measurement serves as a minimum offset. Assuming that the observed displacement has occurred since the formation of the shorelines, which post dates the highstand, we determine a minimum slip rate of 1.4 mm/yr at this site.

a) b)

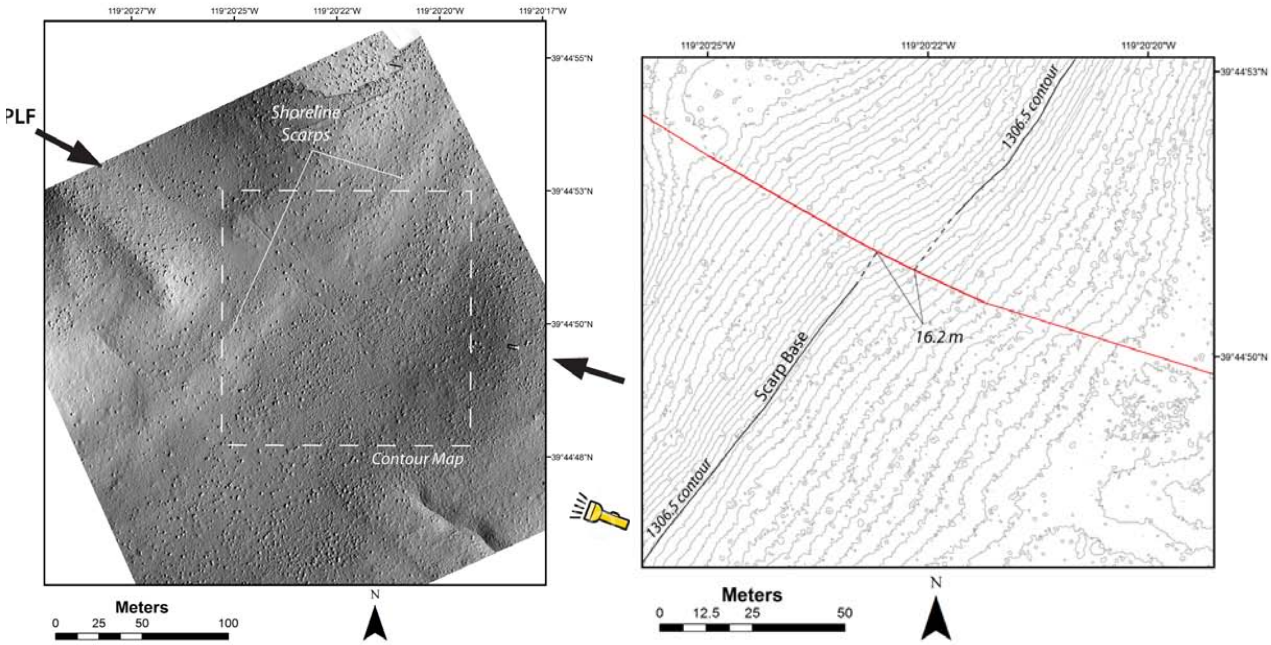

Figure 11. High-resolution model of offset Site 8. a) hillshade model of site showing uphill facing scarp and intersecting shoreline scarps. b) 25cm contour map showing displacement measurement of shorelines (traced with black solid and dotted line).

Discussion

Refinement of the Pyramid Lake fault Slip Rate

The high-resolution models produced in this study provide total of eight new offsets along the northern section of the Pyramid Lake fault. From these observations, we measured right lateral displacements ranging from ~16-25 meters. Combined with lake level studies, we determine a late Pleistocene and Holocene slip-rate ranging from 1.0 - 1.5 mm/yr, with an average rate of 1.3 mm/yr.

This falls within the previously determine slip rate range of 0.7 – 2.6 mm/yr (Briggs and Wesnousky, 2004). We did not, however, observe displacements comparable to the 35 – 42 meters of displacement observed by (Briggs and Wesnousky, 2004), from which the minimum slip rate of 2.6 mm/yr was determined

(Figure 12b). The magnitude of our displacements, however, is comparable to the other displacements they measured (Figure 12a and 12c). The Briggs and Wesnousky (Briggs and Wesnousky, 2004) 35-42 meter displacement is anomalous to all other observed offsets. It occurs ~6km to the south of Site 8 on the southern section of the Pyramid Lake fault, which lies to the south of the east-northeast trending left lateral Olinghouse fault (Figure 3). The presence of the active Olinghouse fault introduces structural and kinematic complexities to fault zone, which may, in part, explain the discrepancies in offset and slip rate observations.

Although the southern section of the fault was not focused on in this study, we provide explanations for the offset and slip rate discrepancies: (1) The southern section of the Pyramid Lake fault is slipping faster than the northern section, and slip is escaping the northern section via the Olinghouse fault. (2) The slip rate is the same, both on the northern and southern sections of the Pyramid Lake fault, and the observed large offset is a result of locally derived high slip rates due to the structural complexities introduced by the proximal Olinghouse fault.

Recent block modeling of the northern Walker Lane using GPS derived velocities determine a slip rate of 1.0 ±0.3 mm/yr on the Pyramid Lake fault (Hammond et al., 2011). The slip rate values determined in this study (1.0 - 1.5 mm/yr) fall within close range of these geodetically derived values.

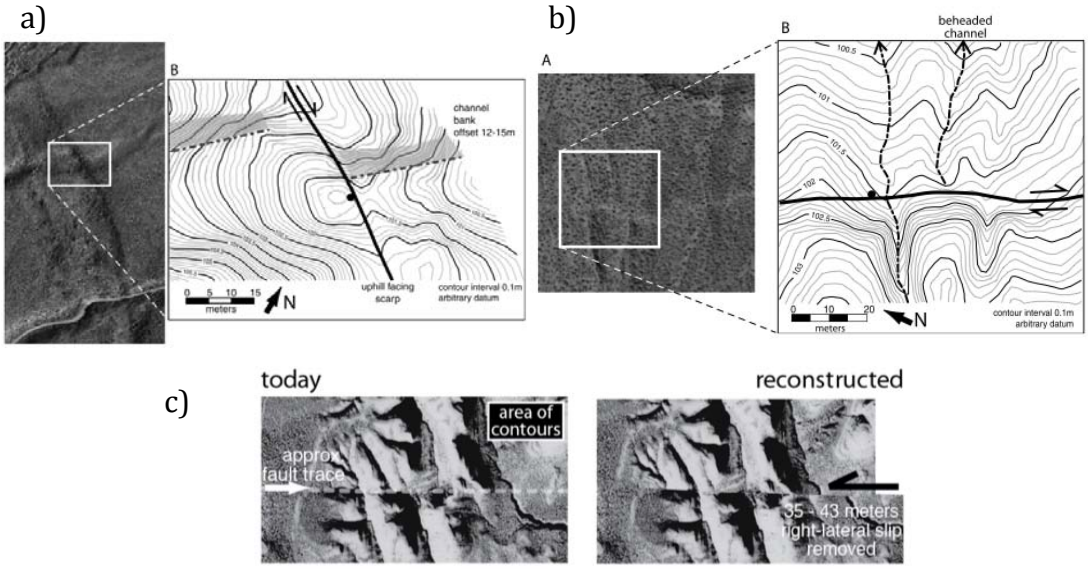

Figure 12. Displacements observed and measured by Briggs and Wesnousky (2004). a) 12-15 meters of right lateral displacement in post-highstand fan (Site 5 in this study). b) 35-43 meters of right lateral displacement in post-highstand drainages. c) 13-15 meters of right lateral displacement of a beheaded channel.

Coeseismic Displacement

Previous paleoseismic trenching across the Pyramid Lake fault have shown evidence for at least four seismic events since the Lohantan highstand (15.5 ka) (Anderson and Hawkins, 1984; Briggs and Wesnousky, 2004). A minimum of two of which post-date the deposition of the Mazama tephra (~7.6 ka) (Briggs and Wesnousky, 2004). Provided the new displacement measurements acquired in this study, the largest measured displacement within post-highstand deposits at Site 2 (24.2 m) suggests average coeseismic displacements of ~6 meters, while average coeseismic displacements of ~4 meters may explain the lowest measured displacement (16.2 meters) at Site 8. Figure 13a shows that these new coeseismic displacements are still larger than would be expected using empirically derived scaling relations for the average slip of a strike-slip fault the length of the Pyramid Lake fault (Wesnousky, 2008). However, they do fall within range of the maximum amount of slip that would be expected for the Pyramid Lake fault (Figure13b).

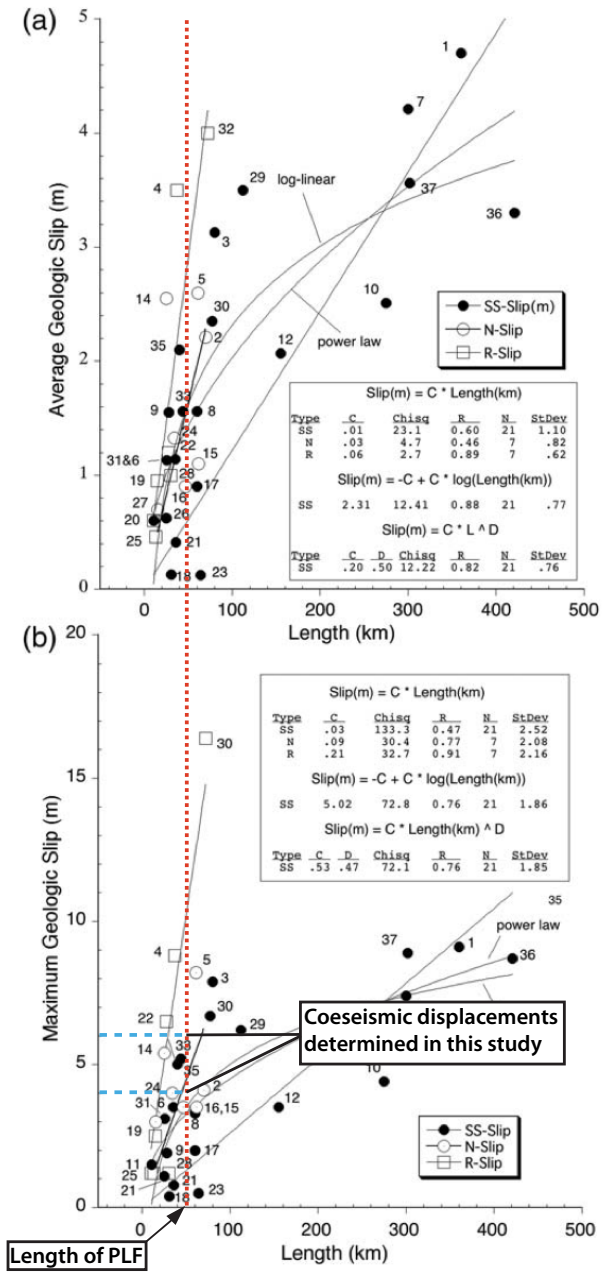

Figure 13. a) Average and b) maximum values of coeseismic surface slip verses length from Wesnousky (2008). Red dotted line plots length of PLF. Blue dashed lines indicate coeseismic values determined in this study.

Conclusion

The high-resolution models produced in this study provide additional measurements of right-lateral displacements along the northern section of the Pyramid Lake fault. From these displacements we determine an average slip rate of 1.3 ±0.3 mm/yr and coeseismic displacements that range from 4-6 meters. These values provide a new independent measurement, which agree with previous observations determined by field mapping methods, albeit it on the low end of this previous range, and also with rates determined from geodetic modeling. Our coseismic values also agree within range of the expected maximum coseismic displacements derived from empirical scaling relations.

References

Adams, K. D., 2012, Response of the Truckee River to lowering base level at Pyramid Lake, Nevada, based on historical air photos and LiDAR data: Geosphere, v. 8, no. 3, p. 607-627.

Adams, K. D., Wesnousky, S. G., and Bills, B. G., 1999, Isostatic rebound, active faulting, and potential geomorphic effects in the Lake Lahontan basin, Nevada and California: Geological Society of America Bulletin, v. 111, no. 12, p. 1739-1756.

Anderson, L. W., and Hawkins, F. F., 1984, RECURRENT HOLOCENE STRIKE-SLIP FAULTING, PYRAMID LAKE FAULT ZONE, WESTERN NEVADA: Geology, v. 12, no. 11, p. 681-684.

Bell, E. J., and Slemmons, D. B., 1979, RECENT CRUSTAL MOVEMENTS IN THE CENTRAL SIERRA NEVADA WALKER LANE REGION OF CALIFORNIA-NEVADA .2. PYRAMID LAKE RIGHT-SLIP FAULT ZONE SEGMENT OF THE WALKER LANE: Tectonophysics, v. 52, no. 1-4, p. 571-583.

Bell, J. W., House, K., and Briggs, R., 2005, Geologic Map of the Nixon Area, Washoe County, Nevada: Nevada Bureau of Mines and Geology.

Benson, L. V., and Thompson, R. S., 1987, LAKE-LEVEL VARIATION IN THE LAHONTAN BASIN FOR THE PAST 50,000 YEARS: Quaternary Research, v. 28, no. 1, p. 69-85.

Briggs, R. W., and Wesnousky, S. G., 2004, Late Pleistocene fault slip rate, earthquake recurrence, and recency of slip along the Pyramid Lake fault zone, northern Walker Lane, United States: Journal of Geophysical Research-Solid Earth, v. 109, no. B8, p. 16.

-, 2005, Late Pleistocene and Holocene paleoearthquake activity of the Olinghouse fault zone, Nevada: Bulletin of the Seismological Society of America, v. 95, no. 4, p. 1301-1313.

Briggs, R. W., Wesnousky, S. G., and Adams, K. D., 2005, Late Pleistocene and late Holocene lake highstands in the Pyramid Lake subbasin of Lake Lahontan, Nevada, USA: Quaternary Research, v. 64, no. 2, p. 257-263.

Eisses, A. K., Kell, A., Kent, G., Driscoll, N., Baskin, R., Smith, K., Karlin, R., Louie, J., and Pullammanappallil, S., in review, New constraints on fault architecture, slip-rates, and strain partitioning beneath Pyramid Lake, Nevada: Geosphere.

Fonstad, M. A., Dietrich, J. T., Courville, B. C., Jensen, J. L., and Carbonneau, P. E., 2013, Topographic structure from motion: a new development in photogrammetric measurement: Earth Surface Processes and Landforms, v. 38, no. 4, p. 421-430.

Hammond, W. C., Blewitt, G., and Kreemer, C., 2011, Block modeling of crustal deformation of the northern Walker Lane and Basin and Range from GPS velocities: Journal of Geophysical Research-Solid Earth, v. 116, p. 28.

Harwin, S., and Lucieer, A., 2012, Assessing the Accuracy of Georeferenced Point Clouds Produced via Multi-View Stereopsis from Unmanned Aerial Vehicle (UAV) Imagery: Remote Sensing, v. 4, no. 6, p. 1573-1599.

Johnson, K., Nissen, E., Saripalli, S., Arrowsmith, J. R., McGarey, P., Scharer, K., Williams, P., and Blisniuk, K., 2014, Rapid mapping of ultrafine fault zone topography with structure from motion: Geosphere.

Sanders, C. O., and Slemmons, D. B., 1996, Geomorphic evidence for Holocene earthquakes in the Olinghouse fault zone, Western Nevada: Bulletin of the Seismological Society of America, v. 86, no. 6, p. 1784-1792.

Snavely, N., Seitz, S. M., and Szeliski, R., 2008, Modeling the world from Internet photo collections: International Journal of Computer Vision, v. 80, no. 2, p. 189-210.

Ullman, S., 1977, STRUCTURE FROM MOTION: Journal of the Optical Society of America, v. 67, no. 10, p. 1400-1400.

-, 1979, INTERPRETATION OF STRUCTURE FROM MOTION: Proceedings of the Royal Society Series B-Biological Sciences, v. 203, no. 1153, p. 405-426.

Wells, D. L., and Coppersmith, K. J., 1994, NEW EMPIRICAL RELATIONSHIPS AMONG MAGNITUDE, RUPTURE LENGTH, RUPTURE WIDTH, RUPTURE AREA, AND SURFACE DISPLACEMENT: Bulletin of the Seismological Society of America, v. 84, no. 4, p. 974-1002.

Wesnousky, S. G., 2008, Displacement and geometrical characteristics of earthquake surface ruptures: Issues and implications for seismic-hazard analysis and the process of earthquake rupture: Bulletin of the Seismological Society of America, v. 98, no. 4, p. 1609-1632.

Westoby, M. J., Brasington, J., Glasser, N. F., Hambrey, M. J., and Reynolds, J. M., 2012, 'Structure-from-Motion' photogrammetry: A low-cost, effective tool for geoscience applications: Geomorphology, v. 179, p. 300-314.